Integrated Regenerative Braking Energy Utilization System for Multi-Substations in Electrified Railways

Junyu Chen, *Student Member, IEEE,* Yinbo Ge, *Student Member, IEEE,* Ke Wang, *Member, IEEE,* Haitao Hu, *Senior Member, IEEE,* Zhengyou He, *Senior Member, IEEE,* Zhongbei Tian, *Member, IEEE, and* Yunwei Li, *Fellow, IEEE*

***Abstract*—This paper proposes an integrated regenerative braking energy utilization system (RBEUS) to improve regenerative braking energy (RBE) utilization in electrified railways. The proposed RBEUS uses a traction substation energy storage system and two sectioning post converters to achieve coordinated RBE utilization in three consecutive traction substations via power-sharing and storage, and the power quality can also be improved. A hierarchically coordinated control strategy is developed based on the operation principle to provide real-time power management and control for the RBEUS. In the system layer, a centralized power management strategy is designed for operation mode management and active power command generation. It uses a sequential quadratic programming-based algorithm to solve the objective function to achieve optimal RBE utilization under different operation modes. In the converter layer, local controllers of the RBEUS enable converters to respond to the active power commands from the system layer and reactive power commands generated by themself for power flow control. The effectiveness of the proposed RBEUS is comprehensively verified by using a hardware-in-the-loop (HIL) experiment. Besides, a comparison analysis of the proposed RBEUS and literature methods is conducted to testify the superiority of the RBEUS. The feasibility of RBEUS implementation is also discussed from fault protection and economy.**

***Index Terms*—regenerative braking energy utilization, electrified railway, hierarchically coordinated control strategy, real-time power management.**

I. INTRODUCTION

ELECTRIFIED railways are one of the most eco-friendly and energy-efficient modes of transportation and have rapidly developed in recent decades. To improve their energy efficiency, regenerative braking has been extensively used in modern trains to generate abundant regenerative braking energy (RBE) during train operation [1]. However, massive RBE is not efficiently utilized within the AC railway power system (RPS) and flows back to the power grid, causing low RBE utilization in the RPS [2], [3]. On the other hand, numerous refluent RBE may aggravate imbalance, harmonics, and catenary voltage fluctuation [4]. As a result, it is meaningful to recycle refluent RBE for energy efficiency and power quality improvement in AC RPS.

Train timetable optimization is a primary attempt, which aims to maximize the RBE utilization by tractive trains in the same power supply section [5], [6]. However, its effect is generally poor due to numerous restraints in the optimization model. With the development of the power electronics techniques, flexible devices, including railway power conditioners (RPCs), energy feedback systems, and energy storage systems (ESSs), have been used to manage the surplus RBE in AC RPS [7]-[9]. Although these devices significantly enhance the controllability of power flow, considerable RBE cannot be used by tractive trains in the RPS due to the limitations in train timetable, device capacity, the segmented structure of the RPS, etc.

In the context of smart grids, the concept of smart railway has been developed to exploit smart electrical infrastructure to achieve high energy efficiency and economical operation of electrified railways [10], [11]. Under this framework, an idea of configuring the smart electrical infrastructure for traction substations (TSSs) and sectioning posts (SPs) along the railway is offered in [12]. This modification connects all segmented power supply sections. As a result, most RBE can be utilized by the tractive trains throughout the railway line, and the surplus RBE is stored in ESSs, achieving more efficient operation [13]. Although this idea is advanced from the scheme perspective, the modification of the RPS throughout the railway line causes complex and expensive transformation and maintenance tasks. Besides, operation control for such a complex system is another critical issue in practical applications.

To control smart electrical infrastructure-based RPS, most studies have focused on the energy management issue from the view of the entire system [14]-[18]. For example, an agent-based railway energy management system was introduced in [14] to coordinate RBE, loads, ESSs, and distributed energy resources along the railway to achieve optimal energy usage. Partial functions have been tested in a real case of the Spanish railway [15]. Based on this concept, a multi-time scale optimal dispatch method is developed for flexible railway energy man-

This work was supported by National Key Research and Development Program of China under Grant 2021YFB2601500, National Natural Science Foundation of China under Grant 52107126, Scientific Foundation for Outstanding Young Scientists of Sichuan under Grant 2021JDJQ0032, and the Fundamental Research Funds for Central Universities under Grant 2682021ZTPY065. (*Corresponding author, Haitao Hu, Ke Wang*).

J. Chen, H. Hu, Y. Ge, K. Wang, and Z. He are with the School of Electrical Engineering, Southwest Jiaotong University, Chengdu 611756, China (e-mail: junyu_chen@my.swjtu.edu.cn; hht@swjtu.edu.cn; GYB@my.swjtu.edu.cn; wangke@swjtu.edu.cn; hezy@swjtu.edu.cn).

Z. Tian is with the Department of Electrical Engineering and Electronics, University of Liverpool, Liverpool, UK, L69 3GJ (e-mail: zhongbei.tian@liverpool.ac.uk).

Y. Li is with the Department of Electrical and Computer Engineering, University of Alberta, Edmonton, AB T6G 2V4, Canada (e-mail: yunwei.li@ualberta.ca)

agement of co-phase RPS integrated with ESSs and renewable energy sources [16]. However, these works focused on optimizing energy scheduling on an operation time scale (i.e., from minutes to days), and the real-time power flow control for electrical infrastructures is not involved.

The real-time control of the electrical infrastructures in the RPS commonly uses communication-based methods to manage the power flow of the modified system due to the distributed nature of the electrified railway. In [19], a two-level charging strategy is designed to coordinate the onboard ESS and wayside ESS to optimize RBE utilization, which decides the optimal power allocation in real-time by a fuzzy logic controller. In addition, a centralized-decentralized control strategy is proposed to improve RBE utilization throughout the railway line by ESS-based electrical infrastructure [20]. However, these publications used rule-based methods that rely on human expertise [21], making it difficult to achieve the optimal power flow management of the modified system. On the other hand, communication-based methods have been applied for coordinating power quality improvement in multiple TSSs. [22] introduced a Steinmetz-based method to generate compensating commands for three RPCs, coordinately controlling them to improve the power quality in three consecutive TSSs. In addition, a method for active power-sharing and reactive voltage support between two adjacent TSSs by the sectioning post converter (SPC) is proposed in [23], and its performance can be improved by integrating a battery-based ESS [24]. Although these methods achieve good performances in power quality improvement, the energy efficiency improvement by RBE utilization is not considered.

This study investigates an integrated regenerative braking energy storage system (RBEUS) for coordinated utilization of the RBE in three consecutive TSSs of electrified railways. It focuses on the real-time power management and control of the RBEUS. Besides, comprehensive experiment verification, comparison analysis, and discussion of practical implementation to support this research are provided. The contributions of this paper are summarized as

1) The proposed RBEUS comprises two SPCs and a traction substation energy storage system (TSESS) to achieve coordinated utilization of the RBE in three consecutive TSSs via power-sharing and storage. The imbalance and catenary voltage fluctuation can also be mitigated by the RBEUS.

2) A hierarchically coordinated control strategy is proposed for the RBEUS, which enables the control system to perform centralized power management in the system layer and decentralized control in the converter layer for real-time control of the RPS integrated with the RBEUS.

3) A power management strategy (PMS) is designed to achieve optimal power management for the RBEUS. It uses the sequential quadratic programming (SQP)-based algorithm to generate active reference powers by solving the operation function for RBE coordinated utilization in the fast and frequent variation of operation conditions with high efficiency.

The remainder of this paper is organized as follows. Section II introduces the RBEUS and its operation principle. Then, Section III proposes the hierarchically coordinated control strategy. Verifications and discussion of the practical implementation of the REBUS are given in Section IV and Section V, respectively. Finally, Section VI concludes the paper.

II. System Description and Operation Principle

A. System Description

Fig.1 shows the architecture of the RPS integrated with the proposed RBEUS. It is installed in three consecutive TSSs, where two SPCs connect two feeders of two adjacent TSSs, and the TSESS connects two feeders of the central TSS. Considering that the storage medium needs to fast and frequently charge or discharge with high power in RPS applications, the supercapacitor is selected as the storage medium for the TSESS [9]. Besides, due to the distributed nature of the electrified railway, the RBEUS requires a communication system to achieve coordinated control of the power flow [10]. The features of the proposed RBEUS are:

1) Coordinated utilization of the RBE: the RBE of each TSS can be transferred by SPCs for adjacent TSS utilization, and the TSESS allows the surplus RBE to be stored and used later. As a result, coordinated utilization of RBE for three TSSs can be achieved by power-sharing and storage of the RBEUS.

2) Power quality improvement: in addition to RBE utilization, the SPC and TSESS can provide additional services such as power factor correction and catenary voltage stabilization [23], [25]. Besides, this configuration helps for imbalance suppression by the alternating phase technique in three consecutive TSSs.

With these features, the RBEUS can comprehensively improve the energy efficiency and power quality of the RPS, and its detailed operation principles are described below.

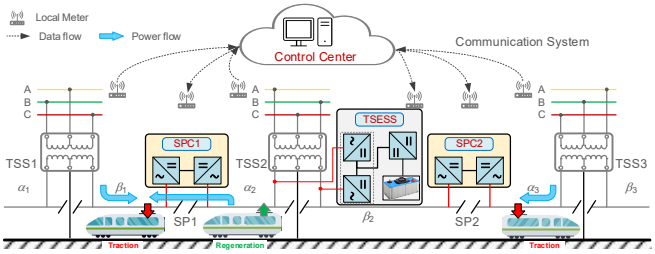

Fig.1 Architecture of three adjacent TSSs integrated with the RBEUS.

B. Operation Principle

1) Coordinated utilization of RBE: In the conventional RPS, neutral zones hinder power-sharing between adjacent sections, which means that the RBE of each TSS has to return to the power grid after tractive train consumption in the same section. Ignoring the power loss of the traction transformer, the active power relation of each TSS is

$$P_{Gi}(t) = P_{Ai}(t) + P_{Bi}(t) + P_{Ci}(t) = P_{\alpha i}(t) + P_{\beta i}(t) \quad (1)$$

where i is the index, and i=1, 2, 3; P_{Gi} is the grid active power of TSS i, which contains two conditions, i.e., draw power from the power grid (P_{Gi}>0) and return regenerative braking power (RBP) to the power grid (P_{Gi}<0); P_A, P_B, P_C, P_α and P_β are active power of phases A, B, C, α, and β, respectively.

As mentioned earlier, the RBEUS realizes RBE utilization in three adjacent TSSs by active power-sharing and storage. In this context, the modified active power relations are derived as

$$P'_{G1}(t) = P_{\alpha 1}(t) + P_{\beta 1}(t) + P_{tr1}(t) \quad (2)$$

$$P'_{G2}(t) = P_{\alpha 2}(t) - P_{tr1}(t) + P_{\beta 2}(t) + P_{tr2}(t) - P_{SC}(t) \quad (3)$$

$$P'_{G3}(t) = P_{\alpha 3}(t) - P_{tr2}(t) + P_{\beta 3}(t) \quad (4)$$

where P'_{Gi} is the modified grid active power of TSS i; P_{tr1} and P_{tr2} are RBP transferred by SPC1 and SPC2, respectively; P_{SC} is the charge/discharge power of the TSESS. Moreover, the positive P_{tr1} and P_{tr2} represent the active power is transferred from the left TSS to the right TSS, and the positive P_{SC} represents the discharge power.

The new power relations in (2)-(4) indicate that RBE utilization among the three TSSs is achieved by transferring the RBE between two adjacent feeders connected by each SPC and storing the surplus RBE by the TSESS for traction consumption. In addition to active power flow dispatch, operational constraints and power loss are required to be considered. Based on (2)-(4), the operation function of the RBEUS for coordinated utilization of RBE can be expressed as

$$f(P_{tr1}(t),P_{tr2}(t),P_{SC}(t))=\sum_{i=1}^{3}|P'_{Gi}(t)|+P_{loss}^{tr}(t)+P_{loss}^{conv}(t) \quad (5)$$

s.t

$$P_{loss}^{tr}(t)=\sum_{j=1}^{2}[(P_{trj}(t)/V_{\alpha j+1})^2\underbrace{r_0 l_{\alpha j+1}}_{R_{\alpha j+1}}+(P_{trj}(t)/V_{\beta j})^2\underbrace{r_0 l_{\beta j}}_{R_{\beta j}}] \quad (6)$$

$$P_{loss}^{conv}(t)=(|P_{tr1}(t)|+|P_{tr2}(t)|+|P_{SC}(t)|(1-\eta_{cd}))(1-\eta_c) \quad (7)$$

$$-S_{spc1}^{N}\le P_{tr1}(t)\le S_{spc1}^{N} \quad (8)$$

$$-S_{spc2}^{N}\le P_{tr2}(t)\le S_{spc2}^{N} \quad (9)$$

$$-P_{SC}^{N}\le P_{SC}(t)\le P_{SC}^{N} \quad (10)$$

$$E_{SC}(t)=P_{SC}(t)\Delta t+(1-\eta_{sds})E_{SC}(t-1) \quad (11)$$

$$SoC(t)=E_{SC}(t)/E_{SC}^{N},SoC_L\le SoC(t)\le SoC_H \quad (12)$$

where P_{loss}^{tr} and P_{loss}^{conv} are transmission loss and power conversion loss, respectively; j is the index; $V_{\alpha j+1}$, $V_{\beta j}$, $R_{\alpha j+1}$, $R_{\beta j}$, $l_{\alpha j+1}$, and $l_{\beta j}$ are catenary voltages, resistances, and lengths of corresponding sections connected by SPCs, respectively; r_0 is unit resistance; η_c and η_{cd} are converter efficiency and charge/discharge efficiency, respectively; η_{sds} is self-discharge coefficient; S_{spc1}^{N}, S_{spc2}^{N}, P_{SC}^{N}, and E_{SC}^{N} are rated capacity of SPCs and TSESS, respectively; SoC is the state of charge of the storage medium; SoC_L and SoC_H are lower and upper limits, respectively.

Equation (5) indicates the real-time power of three TSSs integrated with the RBEUS, which involves the total active power of three TSSs and power loss introduced by the RBEUS. It is only a function of the reference powers for SPCs and TSESS (i.e., P_{tr1}, P_{tr2}, and P_{SC}) because other parameters in the operation function can be pre-obtained or measured in real-time.

2) Power quality improvement: The SPC and TSESS of the RBEUS can be individually used to mitigate power quality issues, which has been comprehensively analyzed in [25], [26]. Specifically, the SPC is usually applied for catenary voltage stabilization [26], which can be expressed as

$$\begin{cases}V_{c\alpha j+1}(t)=(P_{trj}(t)R_{\alpha j+1}+Q_{c\alpha j}(t)X_{\alpha j+1})/V_{\alpha j+1}^{*}(t)\\ V_{c\beta j}(t)=(P_{trj}(t)R_{\beta j}+Q_{c\beta j}(t)X_{\beta j})/V_{\beta j}^{*}(t)\end{cases},j=1,2 \quad (13)$$

where $V_{\alpha j+1}^{*}$, $V_{\beta j}^{*}$, $V_{c\alpha j+1}$, $V_{c\beta j}$, $Q_{c\alpha j}$, $Q_{c\beta j}$, $X_{\alpha j+1}$ and $X_{\beta j}$ separately are targeted voltage, compensation voltage, reactive compensation power, and impedance of corresponding sections, and $X_{\alpha j+1}=x_0 l_{\alpha j+1}$, $X_{\beta j}=r_0 l_{\beta j}$, x_0 is unit impedance.

The TSESS is typically used for imbalance suppression [25], which can be expressed as

$$P_{c\alpha 2}(t)=-P_{c\beta 2}(t)=\frac{(P_{G2}(t)-P_{tr1}(t)-P_{tr2}(t)-P_{SC}(t))}{2} \quad (14)$$

$$\begin{cases}Q'_{c\alpha 2}(t)=Q_{\alpha 2}(t)+Q_{c\alpha 2}(t)-P_{c\alpha 2}(t)\tan(30^\circ)/2\\ Q'_{c\beta 2}(t)=Q_{\beta 2}(t)+Q_{c\beta 1}(t)-P_{c\beta 2}(t)\tan(30^\circ)/2\end{cases} \quad (15)$$

where $P_{c\alpha 2}$, $P_{c\beta 2}$, $Q'_{c\alpha 2}$ and $Q'_{c\beta 2}$ separately are active power and reactive power compensated by the TSESS for α and β phase of TSS2.

Based on the operation principles of the RBEUS, RBE utilization in three consecutive TSSs relies on the power flow coordinated control of SPCs and TSESS, while power quality improvement depends on the individual control of SPCs and TSESS. As a result, an effective control strategy is required for coordinating RBEUS operation.

III. Hierarchically Coordinated Control Strategy

To effectively control the RBEUS, two critical components must be included: 1) a system-level PMS to manage the active power flow of the modified system, and 2) converter-level control strategies to execute power commands generated by the PMS. Thus, a hierarchically coordinated control strategy is proposed to address these issues, as shown in Fig.2.

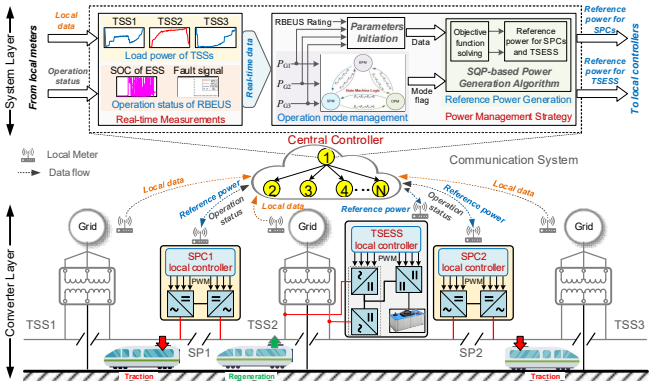

Fig.2 Proposed hierarchically coordinated control strategy for RBEUS.

In the system layer, a real-time PMS is executed in the central controller to generate active reference powers based on local meter data. Local controllers of SPCs and TSESS respond to reference powers generated by the central controller to achieve active power flow control in the converter layer. Local controllers also generate reactive reference powers for power quality improvement. Besides, the communication impact on the hierarchically coordinated control strategy is considered. Details of each layer are presented in the following subsections.

A. System Layer

The system layer executes the system-level PMS to realize operation mode management and active reference power generation based on the local meter data. The proposed PMS is shown in Fig.3, which has the following objectives: 1) decide the operation mode of the RBEUS based on the operation condition of three TSSs; 2) achieve seamless transition of different operation modes; 3) generate reference powers for SPCs and TSESS to coordinate RBE utilization among three TSSs.

For the first two objectives, the operation modes are first analyzed based on the operation conditions of three TSSs. Three operation modes can be classified based on the total grid

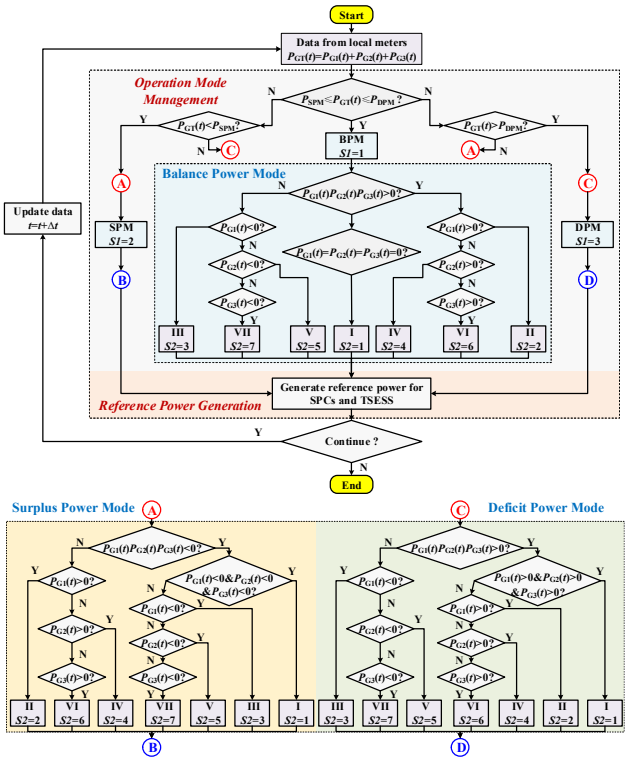

Fig. 3 Proposed PMS for the RBEUS.

active power of three TSSs (P_{GT}=P_{G1}+P_{G2}+P_{G3}): 1) *surplus power mode* (SPM, P_{GT}<P_{SPM}); 2) *deficit power mode* (DPM, P_{GT}>P_{DPM}); 3) *balance power mode* (BPM, P_{SPM}≤P_{GT}≤P_{DPM}). P_{SPM} and P_{DPM} are the power thresholds for SPM and DPM, respectively, which are preferred to be negative and positive rather than zero and can be set as the no-load power of the RPS to avoid fluctuation in the mode switch. Different condition combinations of three TSSs can also achieve the same P_{GT} due to P_{Gi} has two power directions, i.e., P_{Gi} >0 or P_{Gi} <0, which means that several scenarios exist in each mode. The detailed classification of operation modes and scenarios is depicted in Fig.3. *S1* is the mode flag to decide the operation mode by power thresholds, and *S2* is the scenario flag to determine the operation scenario based on the power directions of three TSSs. The operation principles of each mode are:

1) SPM (P_{GT}<P_{SPM}): In this mode, the available RBP is greater than the tractive power demand, and P_{GT} is less than the P_{SPM}. The storage medium stores surplus RBP after the RBP is transferred by SPCs for traction utilization. Once SoC reaches the upper limit, surplus RBP is sent to the power grid. As shown in Fig.3, this mode has seven scenarios, and their reference powers for SPCs and TSESS are calculated by a reference power generation algorithm introduced later.

2) DPM (P_{GT}>P_{DPM}): In DPM mode, the available RBP is less than the tractive power demand, and P_{GT} is greater than P_{DPM}. The storage medium supplies deficit tractive power for TSSs, and the discharge threshold can be set to reduce the peak power demand [25]. Once the SoC reaches the lower limit, the supercapacitor becomes idle, and the power grid supplies the active power for TSSs. Similar to the SPM, the DPM also contains seven scenarios, and their reference powers for SPCs and TSESS are calculated by the same algorithm for the SPM.

3) BPM (P_{SPM}≤P_{GT}≤P_{DPM}): The BPM indicates that P_{GT} is between two power thresholds, which means that only SPCs transfer RBE for utilization, and the supercapacitor is idle. Therefore, the reference power of the TSESS is zero, and the reference powers for SPCs under each scenario can be obtained by the same algorithm for the SPM and DPM.

According to the operation modes and scenarios in Fig.3, the first two objectives of the PMS can be achieved via the state machine logic, which is easy to implement to manage the fast and frequent variations in operation modes and scenarios with high efficiency [9]. For the last objective, it can be realized by solving the operation function of (5). To maximize the grid active power reduction of the three TSSs by the RBEUS, the minimum value of (5) is required to be achieved by solving the optimal P_{tr1}, P_{tr2}, and P_{SC}. Consequently, the objective function can be derived as

$$\min f(\mathbf{x})=\sum_{i=1}^{3}|P'_{Gi}(t)|+P_{loss}^{tr}(t)+P_{loss}^{conv}(t) \tag{16}$$

s.t

$$\begin{cases} h(\mathbf{x})=0 \\ g(\mathbf{x})\le 0 \end{cases} \tag{17}$$

where $\mathbf{x}$ is the variable vector, and $\mathbf{x}$=[x_1, x_2, x_3]'=[$P_{tr1}(t)$, $P_{tr2}(t)$, $P_{SC}(t)$]'; $h(\mathbf{x})$ and $g(\mathbf{x})$ separately are the equality and inequality constraints derived from (8)-(12), which are given in the Appendix.

However, the objective function is highly nonlinear, including several absolute values and quadratic terms, which needs a complex solving technique and increases the computational burden for the central controller. Thus, an SQP-based reference power generation algorithm is proposed, which is shown in Fig.4. The algorithm first simplifies the objective function as a standard quadratic programming problem under each known operation mode and scenario and then solves this problem using the SQP algorithm. The SQP algorithm is a gradient search method with a superb performance in accuracy, convergency, and efficiency, and it thus has been used to address optimization issues for real-time applications [27].

According to Fig.4, the procedure of the proposed SQP-based reference power generation algorithm is summarized as:

Step1: Input real-time measured grid active powers, catenary voltage, SoC, operation mode, and scenario.

Step2: Initialize system parameters, such as converter ratings, SoC limits, unit resistance, line distance, and related temporary variables.

Step3: Formulate the objective function as (16) based on the inputs and initialization, then simplify it based on the operation mode and scenario. Specifically, the operation mode flag *S1* can determine the sign of P_{SC} and the operation scenario flag *S2* can decide the sign of P'_{Gi}, P_{tr1}, and P_{tr2}. For example, when *S1*=3 and *S2*=1, P_{Gi} >0, thus P'_{Gi} >0, P_{tr1}<0, P_{tr2}>0, P_{SC}>0. Then the absolute values of (16) are simplified, and a standard quadratic objective function is obtained.

Step4: Generate the reference powers by the SQP algorithm. The SQP algorithm formulates the Hessian matrix (i.e., $\mathbf{H}^k$) at the kth iteration, and then it is invoked to iteratively solve the quadratic subproblem of the optimization problem (i.e., Eq.(18)) under corresponding constraints (i.e., Eq.(19)) until the result is con-

verged [28]. The whole solving progress of the SQP algorithm can be expressed as

$$\min_{\mathbf{d}\in\mathbb{R}^n} \nabla f(\mathbf{x}^k)^{\mathrm{T}}\mathbf{d} + \frac{1}{2}\mathbf{d}^{\mathrm{T}}\mathbf{H}^k\mathbf{d} \tag{18}$$

s.t

$$\begin{cases} \nabla h(\mathbf{x}^k)^{\mathrm{T}}\mathbf{d} + h(\mathbf{x}^k) = 0 \\ \nabla g(\mathbf{x}^k)^{\mathrm{T}}\mathbf{d} + g(\mathbf{x}^k) \le 0 \end{cases} \tag{19}$$

where ∇ denotes the gradient; $\mathbf{d}$ is the search direction and $\mathbf{d} = \mathbf{x} - \mathbf{x}^k$; $\mathbf{H}$ is the Hessian matrix, and $\mathbf{H}^k = \nabla^2 f(\mathbf{x}^k)$; k is the iterative index; $h(\mathbf{x}^k)$ and $g(\mathbf{x}^k)$ separately are the equality and inequality constraints at kth iteration. The expressions of $h(\mathbf{x}^k)$, $g(\mathbf{x}^k)$, $\nabla h(\mathbf{x}^k)$, $\nabla g(\mathbf{x}^k)$ and $\mathbf{H}^k$ are given in the Appendix.

Algorithm: SQP-based Reference Power Generation

1 ***Input:***
Real-time local meter data: P_{G1}, P_{G2}, P_{G3}, $V_{\beta 1}$, $V_{\alpha 2}$, $V_{\beta 2}$, $V_{\alpha 3}$, SoC;
Operation mode and scenario flag: *S1*, *S2*;

2 ***Initialization:***
Parameters: $P_{\mathrm{SC}}^{\mathrm{N}}$, $E_{\mathrm{SC}}^{\mathrm{N}}$, $\mathrm{SoC_H}$, $\mathrm{SoC_L}$, $S_{\mathrm{spc1}}^{\mathrm{N}}$, $S_{\mathrm{spc2}}^{\mathrm{N}}$, $l_{\beta 1}$, $l_{\alpha 2}$, $l_{\beta 2}$, $l_{\alpha 3}$, r_0, η_{sds}, η_{c}, η_{cl};
Variables: k=0, ε=0.0001, $\mathbf{x_0}$=[0, 0, 0]', $P_{tr1} \in [-S_{\mathrm{spc1}}^{\mathrm{N}}, S_{\mathrm{spc1}}^{\mathrm{N}}]$, $P_{tr2} \in [-S_{\mathrm{spc2}}^{\mathrm{N}}, S_{\mathrm{spc2}}^{\mathrm{N}}]$, $P_{\mathrm{SC}} \in [-P_{\mathrm{SC}}^{\mathrm{N}}, P_{\mathrm{SC}}^{\mathrm{N}}]$;

3 ***Formulation and simplification for the objective function:***

4 Formulate the objective function based on inputs and initialization;

5 Update the range of P_{SC} based on *S1*: ***if*** *S1*==1, ***then*** $P_{\mathrm{SC}} \in [-P_{\mathrm{SC}}^{\mathrm{N}}, 0]$; ***if*** *S1*==2, ***then*** $P_{\mathrm{SC}} \in [0, P_{\mathrm{SC}}^{\mathrm{N}}]$; ***if*** *S1*==0, ***then*** $P_{\mathrm{SC}} = 0$;

6 Simplify the absolute values of P_{loss}^{conv} by the modified range of P_{SC};

7 Simplify the absolute values of (16) based on the power directions sign of grid active power of three TSSs, i.e., *S2*;

8 Formulate the standard quadratic objective function based on the simplified objective function of (16): **min** $f(\mathbf{x})$=$f(P_{tr1}, P_{tr2}, P_{\mathrm{SC}})$;

9 ***Solving the objective function by SQP:***

10 Iteration for solving the objective function by SQP;

11 ***if*** $\|\mathbf{d}^k\|<\varepsilon$, ***then*** $\mathbf{x}^*=\mathbf{x}^k$, $f(\mathbf{x}^*)$=$f(\mathbf{x}^k)$, and go to step 12
Otherwise, set k=k+1, update $\mathbf{x}^{k+1}$=$\mathbf{x}^k$+$\mathbf{d}^k$, $\mathbf{H}^{k+1}$ and return to step 10;

12 Return optimal reference power: $[P_{tr1}^*, P_{tr2}^*, P_{\mathrm{SC}}^*] = \mathbf{x}^*$;

Fig.4 Illustration of SQP-based reference power generation algorithm.

According to the SQP-based reference power generation algorithm of Fig.4, the last objective of the PMS is achieved. These generated active reference powers are sent from the central controller to local controllers of SPCs and TSESS for converter control, which is discussed in the following subsection.

B. Converter Layer

The converter layer involves control strategies for SPCs and TSESS of the RBEUS, which tracks reference powers to control the power flow of the RPS.

1) *Control strategy for SPCs:* SPCs adopt the back-to-back topology to transfer power between two feeders of two adjacent TSSs. The overall control strategy for SPCs is depicted in Fig.5. To ensure SPC performance, the control strategy must stabilize DC bus voltage and track reference powers. As a result, the left converter of the SPC uses cascaded dual-loop control to control the DC bus voltage and reference powers. For the power control, it is transformed as the current control and realized by the proportional resonant (PR) controller. With a stable DC bus, the right converter of the SPC only requires current control to track the reference current by the PR controller. The active reference powers for SPCs are obtained from the central controller, and the corresponding reference power for each converter of the SPC is

$$P_{\mathrm{SPC}j\mathrm{L}}^*(t) = -P_{\mathrm{SPC}j\mathrm{R}}^*(t) = P_{trj}^*(t), j = 1,2 \tag{20}$$

Besides, the SPCs can compensate for reactive power for catenary voltage support [26], which can be derived from (13) as

$$\begin{cases} Q_{\mathrm{SPC}j\mathrm{L}}^*(t) = (V_{c\alpha j+1}^*(t)V_{\alpha j+1}(t) - P_{trj}(t)R_{\alpha j+1}) / X_{\alpha j+1} \\ Q_{\mathrm{SPC}j\mathrm{R}}^*(t) = (V_{c\beta j}^*(t)V_{\beta j}(t) - P_{trj}(t)R_{\beta j}) / X_{\beta j} \end{cases}, j = 1,2 \tag{21}$$

where $V_{c\alpha j+1}^*$ and $V_{c\beta j}^*$ separately are targeted compensation voltage of corresponding sections, and $V_{c\alpha j+1}^* = V_{\alpha j+1}^* - V_{\alpha j+1}$, $V_{c\beta j}^* = V_{\beta j}^* - V_{\beta j}$.

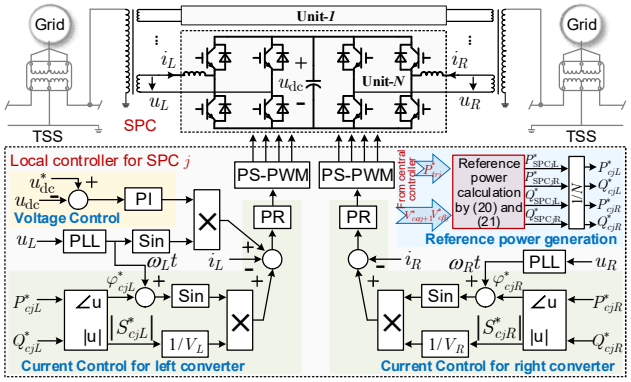

Fig.5 Control diagram of SPCs.

2) Control strategy for TSESS: The TSESS is a back-to-back converter-based ESS that integrates a supercapacitor-based ESS (SCESS) at the DC bus of the back-to-back converter. For such a multi-converter system, coordinated control for these converters is essential. Thus, the control objective of each converter can be determined: (i) the left converter of the back-to-back converter provides DC bus voltage regulation; and (ii) the remaining converters provide power regulation [9]. According to these control objectives, the control strategy can be formulated, as shown in Fig.6. Specifically, the control strategy for the back-to-back converter is the same as that for the SPCs. SCESS uses current control to track the charge or discharge power of supercapacitors. Based on (14) and (15), the active reference power for each converter can be derived as

$$\begin{cases} P_{\mathrm{TSESSL}}^*(t) = (P_{\alpha 2}(t) - P_{tr1}(t) - P_{\beta 2}(t) - P_{tr2}(t) - P_{\mathrm{SC}}(t))/2 \\ P_{\mathrm{TSESSR}}^*(t) = (P_{\beta 2}(t) + P_{tr2}(t) - P_{\alpha 2}(t) + P_{tr1}(t) - P_{\mathrm{SC}}(t))/2 \\ P_{\mathrm{SCESS}}^*(t) = P_{\mathrm{SC}}^*(t) \end{cases} \tag{22}$$

In addition, the back-to-back converter of the TSESS can compensate for the reactive power for power factor improvement, particularly for imbalance suppression [25]. The reactive reference powers can be derived from (15) as

$$\begin{cases} Q_{\mathrm{TSESSL}}^*(t) = Q_{\alpha 2}(t) + Q_{c\alpha 2}(t) - P_{\mathrm{G2}}'(t)\tan(30^\circ)/2 \\ Q_{\mathrm{TSESSR}}^*(t) = Q_{\beta 2}(t) + Q_{c\beta 1}(t) - P_{\mathrm{G2}}'(t)\tan(30^\circ)/2 \end{cases} \tag{23}$$

C. Communication Impact

The proposed hierarchically coordinated control strategy is a communication-based method, which decides the coordinated control of SPCs and TSESS for RBE utilization. Therefore, the communication impact on the proposed control strategy is considered, including the communication delay and fault [29].

1) Communication delay: Communication delay is inevitable, which causes a time delay in load power acquisition of central controller and power command acquisition of local controllers. However, this issue does not impact the stability of

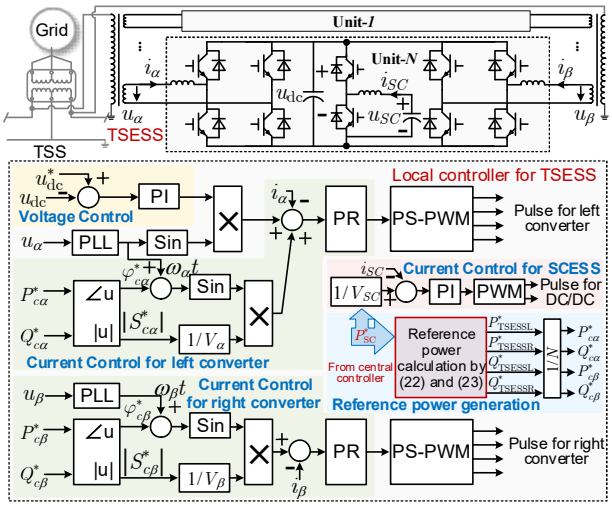

Fig.6 Control diagram of the TSESS.

the control system due to the converter control only depends on its local controllers, and time delay only causes power commands to be delayed. In normal conditions, the time delay of communication systems along modern railways has been satisfied the requirement of real-time control [30]. Since the executime of the system layer and converter layer control is several milliseconds, the entire execution time of the hierarchical control strategy with considering the communication delay is far shorter than the variation of load powers. In extreme conditions, a long time delay (such as several seconds or even longer) can be addressed by the communication protection, which will clear the power commands in the local controller to avoid the mismatch between power commands and load power.

2) Communication fault: The communication fault will cause different impacts on the TSESS and SPCs. Since the load power cannot be measured at SPs, the active reference powers for SPCs rely on the central controller. If a communication fault occurs, the SPCs will standby and not output power. For the TSESS, it can individually operate for RBE utilization and power quality improvement of the TSS without communication due to the load power can be measured at the TSS.

IV. VERIFICATION

This section uses two cases to verify the proposed RBEUS and hierarchically coordinated control strategy. The first case validates the effectiveness of the proposed RBEUS and the coordinated control strategy under all operation modes. On this basis, the second case evaluates the performance of the proposed RBEUS through a comparison analysis between the RBEUS and existing schemes.

A. Experimental Result

This case tests the proposed RBEUS and coordinated control strategy under all operation modes and seamless transition among all modes based on the hardware-in-the-loop (HIL) experiment. Fig.7 shows the details of the HIL experimental platform, which contains an OPAL-RT 5700 real-time simulator (a Xilinx Virtex-7 FPGA with 32 of Intel Xeon processing cores), an external digital controller (a Xilinx XC6SLX16 and a TI TMS320C28346), and a host computer. Specifically, the circuit model of three TSSs with the RBEUS and local controllers are built in different cores of real-time simulator by RT-LAB

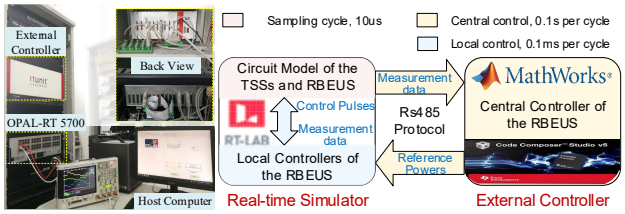

Fig.7 HIL experimental platform for the RPS equipped with the RBEUS: (a) physical plant; (b) detailed implementation.

TABLE I
PARAMETERS OF THE EXPERIMENT PLATFORM

Items	Parameters	Value
TSSs	V/v transformer ratio	110kV/27.5kV
	V/v transformer capacity	50MVA
	Line impedance	0.078+0.62j Ω/km
	Section length $l_{\beta 1}$, $l_{\alpha 2}$, $l_{\beta 2}$, $l_{\alpha 3}$	9, 10, 11, 10km
SPCs and TSESS	Isolated transformer ratio	27.5kV/1500V
	Isolated transformer capacity	6MVA
	S^{N}_{spc1}, S^{N}_{spc2}	6MVA
	P^{N}_{SC}, E^{N}_{SC}	4MW, 200kWh
	P_{SPM}, P_{DPM}	-0.3MW, 0.3MW
	Leg inductor	1mH
	DC bus Capacitor	10mF
	DC bus reference value	3600V
	SCESS converter inductor	3mH
	Lower and upper limit of SoC	0.05, 0.95
	Efficiency η_c, η_{cd}	97.8%, 98%
	Self-discharge coefficient η_{sds}	20% /day
	Communication delay	30ms

TABLE II
EXPERIMENTAL CONDITIONS AND CORRESPONDING RESULTS

Mode and Scenario		Active power of each TSS(MW)						$\sum_{i=1}^{3}\lvert P_{Gi}\rvert$	$\sum_{i=1}^{3}\lvert P'_{Gi}\rvert$	P_{loss} (MW)
		P_{G1}	P'_{G1}	P_{G2}	P'_{G2}	P_{G3}	P'_{G3}			
SPM	I	-4	-1.95	-2	0.17	-1	-1	7	**3.12**	0.21
	II	1	0.02	-4	0.17	-3	-1.98	8	**2.17**	0.21
	III	-7	-0.79	2	0.08	2	0.05	11	**0.93**	0.34
	IV	-1	0.02	1	0.17	-4	0.12	6	**0.31**	0.31
	V	3	0.08	-6	0.08	1	0.02	10	**0.19**	0.19
	VI	-3	-0.95	-3	0.17	1	0.02	7	**1.14**	0.24
	VII	2	0.05	2	0.08	-7	-0.79	11	**0.93**	0.34
DPM	I	2	0.05	1	0.17	2	1.02	5	**1.24**	0.24
	II	7	1.21	-1	0.17	-1	0.02	9	**1.40**	0.40
	III	-2	0.05	5	0.17	2	1.02	9	**1.24**	0.24
	IV	-1	0.02	4	0.08	-1	0.02	6	**0.13**	0.13
	V	1	0.02	-2	0.17	6	1.16	9	**1.35**	0.35
	VI	-1	0.02	-1	0.08	4	0.12	6	**0.23**	0.23
	VII	3	1.05	4	0.17	-2	0.05	9	**1.27**	0.27
Seamless transfer	SPM	-7	-0.79	2	0.12	1	0.02	10	**0.94**	0.36
	BPM	-2	0.05	3	0.00	-1	0.02	6	**0.08**	0.08
	DPM	2	1.03	6	0.17	-3	0.08	11	**1.28**	0.27
	SPM	2	0.05	1	0.12	-6	0.21	9	**0.38**	0.38
	DPM	7	1.21	-1	0.17	-1	0.02	9	**1.40**	0.40
	BPM	5	0.16	-3	0.00	-2	0.05	10	**0.21**	0.21
	SPM	2	0.05	-8	-0.83	1	0.02	11	**0.91**	0.24

software with MATLAB. The external digital controller executes the central controller codes generated by MATLAB Coder with the TI C2000 package under the Code Composer Studio environment. During operation, the external controller generates active reference powers based on the local data from

TSSs and RBEUS, and then it sends them back to the real-time simulator to coordinately control the RBEUS. In this way, the modified system can be accurately reproduced in the real-time simulator, together with the external controller, providing comprehensive tests for system functions. The detailed platform parameters and experimental conditions are listed in Tables I and II.

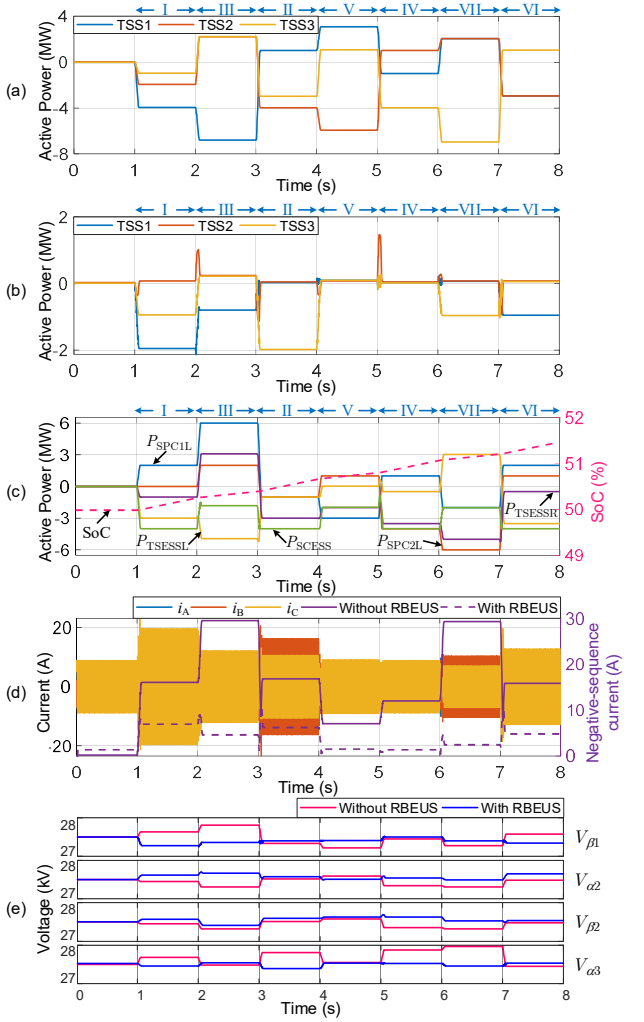

Fig. 8 Experimental results of SPM: (a) grid active power without RBEUS; (b) grid active power with RBEUS; (c) RBEUS; (d) three-phase and negative-sequence current; (e) catenary voltage.

1) Performance under SPM: Seven scenarios of the SPM are tested in this case. The experimental conditions of each scenario are shown in Table II, and the experimental results are shown in Fig.8. Fig.8(a) and Fig.8(b) depict the active power of three TSSs with and without the RBEUS, and detailed results are given in Table II. In this case, the load powers of the three TSSs change every second with a step variation, as shown in Fig.8(a). The returned RBP in each scenario is shown to decrease markedly when transferred to the adjacent TSS for tractive power consumption and energy storage, as depicted in Fig.8(b). The RBEUS changes power with the scenario switch, and the SoC of the supercapacitor increases with storing RBP, as shown in Fig.8(c). Fig.8(d) and (e) show the rms values for negative-sequence current and catenary voltage. The negative-sequence current of the common coupling point is suppressed, and the voltages of the catenary connected by RBEUS are stabilized. Besides, communication delay causes transient phenomenon for output powers of the RBEUS when load powers variation, but all scenarios realize the seamless transition. As shown in Table II, although slight power loss exists, the grid active powers of three TSSs are significantly decreased. Thus, the RBE utilization rate and power quality are improved.

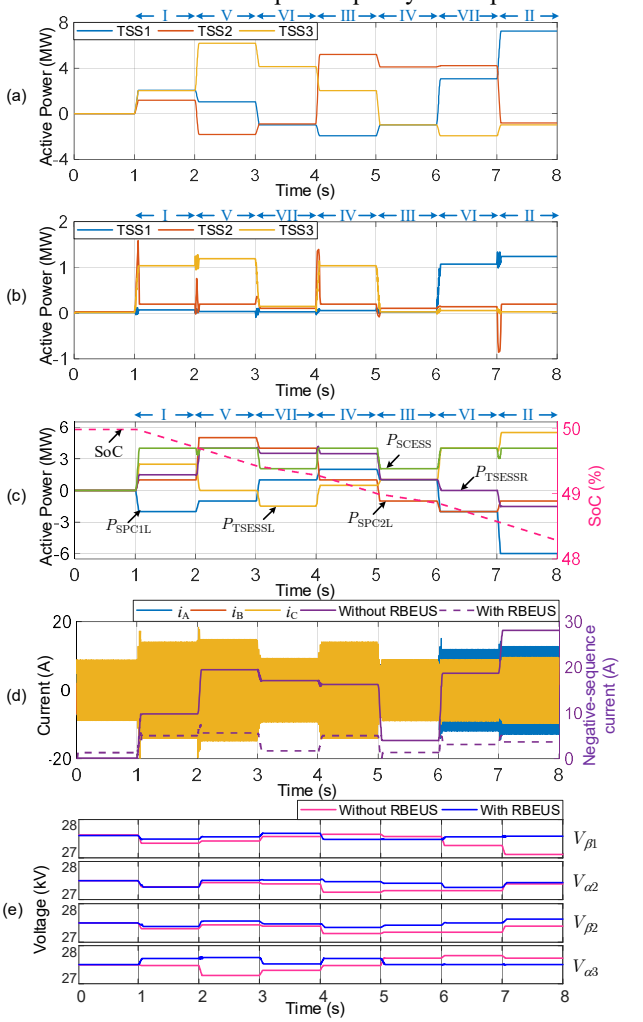

Fig. 9 Experimental results of DPM: (a) grid active power without RBEUS; (b) grid active power with RBEUS; (c) RBEUS; (d) three-phase and negative-sequence current; (e) catenary voltage.

2) Performance under DPM: Fig.9 depicts the experimental results of DPM based on the experimental conditions of Table II. Fig.9(a)-(c) and Table II show that the tractive power and backflow RBP in each scenario are markedly decreased, owing to the RBP of adjacent TSSs and stored RBP of the supercapacitor are transferred for utilization. During DPM operation, the SoC decreases with releasing the stored RBP, as depicted in Fig.9(c). Besides, power quality issues, including negative-sequence current and catenary voltage fluctuation, are alleviated, as shown in Fig.9(d) and (e). Although the communication delay leads to a transient phenomenon when operation scenario switch, seamless transition throughout the operation scenarios of DPM shows good performance in RBE utilization and power quality improvement during operation.

3) Performance under the seamless transition of different modes: This case presents the performance of the RBEUS in the seamless transition among different modes. Table II lists

the experimental conditions, and the corresponding results are presented in Fig.10. The load powers of the three TSSs are changed every second, causing the RBEUS to switch operation mode between the SPM, DPM, and BPM seamlessly, as shown in Fig.10(a)-(e). Fig.10 and Table II show that the grid active powers of the three TSSs in each mode are decreased due to the RBE utilization, including tractive power and feedback RBP. In addition, the SoC varies with the operation mode of the RBEUS, as shown in Fig.10(c). Regarding power quality, the negative-sequence current and catenary voltage fluctuation are suppressed, as shown in Fig.10(d) and (e). In addition, the transient phenomenon caused by communication delay does not affect the stable operation of the RBEUS.

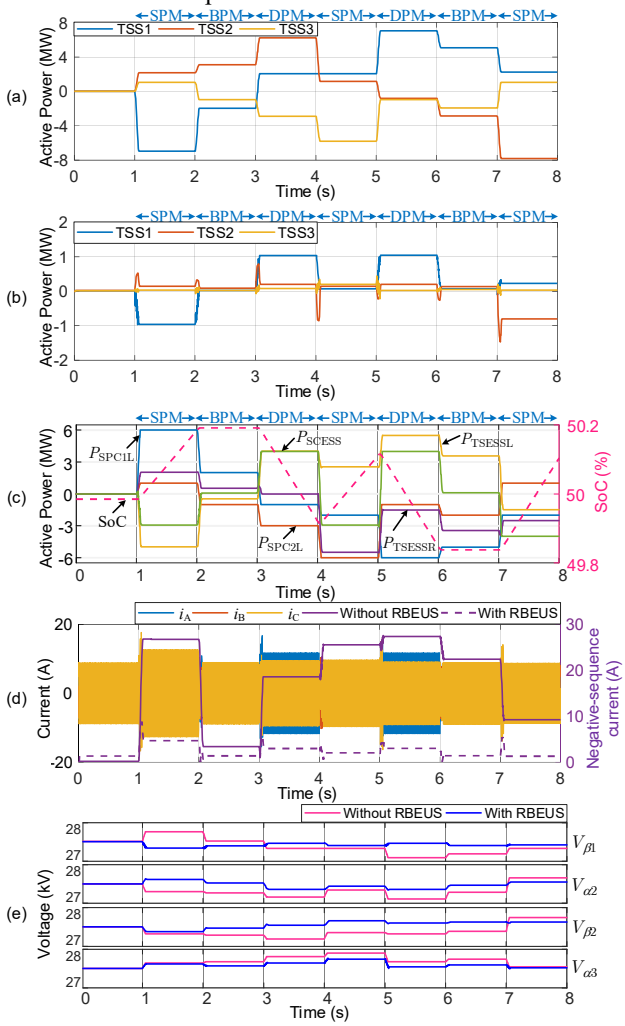

Fig. 10 Experimental results of seamless transition among all modes: (a) grid active power without RBEUS; (b) grid active power with RBEUS; (c) RBEUS; (d) three-phase and negative-sequence current; (e) catenary voltage.

4) Performance under extreme communication delay and communication fault: The extreme communication delay can be considered a typical case of communication fault, and only communication fault condition is tested here. The experimental conditions are selected from the first two conditions of the seamless transition case, and the results are shown in Fig.11. The RBEUS normally operates for RBE coordinated utilization in three TSSs at the beginning, and the communication fault occurs at t=1.5s. As shown in Fig.11(c), two SPCs stop operating due to the communication fault is detected by their local controllers, and the TSESS still operates normally for RBE utilization in TSS2 by its local controller. When t=2.5s, the communication is resumed. The SPCs restart to transform active power between adjacent TSSs, and the TSESS changes operation status to manage the new active power flow. Thus, the RBEUS continues to be coordinately controlled by the power commands from the central controller after the communication fault recovery.

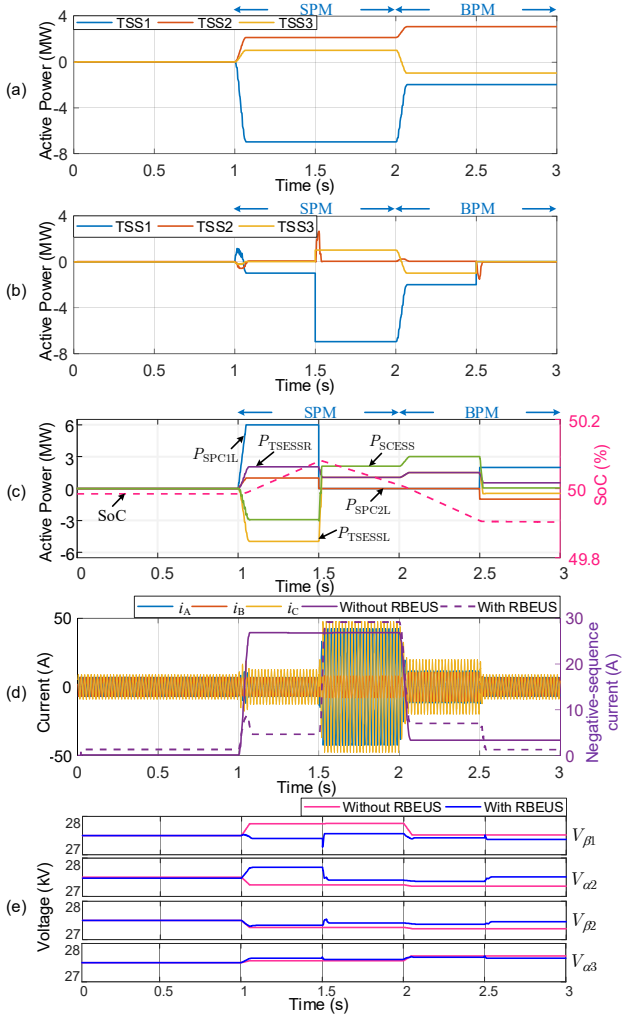

Fig. 11 Experimental results of communication fault: (a) grid active power without RBEUS; (b) grid active power with RBEUS; (c) RBEUS; (d) three-phase and negative-sequence current; (e) catenary voltage.

Based on the above experimental results, we can conclude:

1) Although slight power loss exists, the grid active power of each TSS, including the tractive power and returned RBP, is significantly decreased by transferring RBE for traction utilization and recycling RBE by the storage medium. Thus, the energy efficiency of the RPS is improved by the RBEUS.

2) Although communication delay causes transients when the operation condition switches, the negative-sequence current of the common coupling point and the catenary voltage fluctuation are still alleviated. Therefore, the power quality of the RPS is improved by the RBEUS.

3) The proposed coordinated control strategy for the RBEUS shows good performance when managing with the fast and frequent variation of operation conditions, achieving the

seamless transition under different modes with high efficiency. The proposed strategy implements RBEUS control well, even during communication delays and fault conditions.

B. Comparison of Various Methods

In this case, the proposed RBEUS is compared with the existing schemes based on the field load data of three adjacent TSSs in the Shenshuo heavy haul railway. The three TSSs locate on a long downhill area and return approximately 30 MWh RBE daily to the power grid. The parameters of the SPC and TSESS for these schemes are based on Table I, and the results are shown in Fig.12 and Table III.

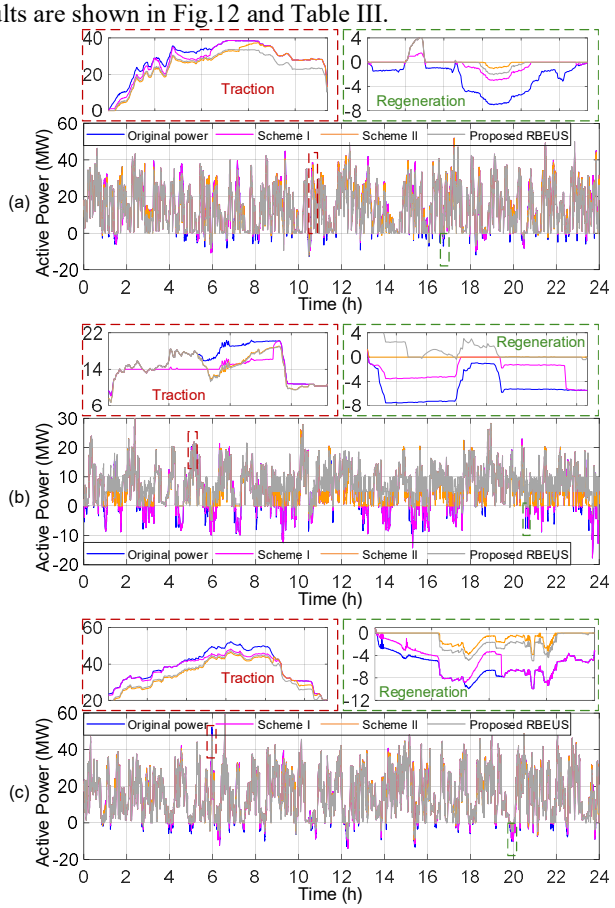

Fig.12 Comparison between conventional ESS scheme and proposed RBEUS: (a) TSS1; (b) TSS2; (c) TSS3.

Scheme I installs a TSESS in each TSS for RBE utilization. The returned RBE and tractive energy of the three TSSs decreases by 9.7MWh and 6.1MWh, accounting for about 31.1% and 0.6%, respectively. It thus reduces about 0.7MW maximum power demand. Due to the back-to-back converter of the TSESS balances the tractive power of two feeders when there is no RBE, additional power conversion loss occurs. Thus, this scheme yields about 3.6MWh energy loss.

Scheme II employs two SPCs and three TSESS to connect all sections of three TSSs and achieves the best effect in RBE utilization of three schemes (about 95.2%). However, its PMS allows it to exchange power with all sections of three TSSs, leading to more energy loss than Scheme I. Consequently, the tractive energy reduction of this scheme is about 23.8MWh (about 2.5%). Besides, this scheme realizes a better effect in maximum power demand reduction than Scheme I by power-sharing among three TSSs (about 1.3MW).

TABLE III
DETAILED COMPARISON RESULTS

Indicators		Original RPS	Scheme I [9]	Scheme II [20]	Proposed RBEUS
Tractive energy (MWh)	TSS1	392.5	390.6	379.7	373.9
	TSS2	160.3	158.4	153.6	161.9
	TSS3	386.5	384.2	382.2	377.3
	Total	**939.3**	**933.2**	**915.5**	**913.1**
Returned RBE (MWh)	TSS1	6.4	3.1	0.8	1.3
	TSS2	17.5	14.6	0.2	0.4
	TSS3	7.3	3.8	0.5	1.4
	Total	**31.2**	**21.5**	**1.5**	**3.1**
Maximum Power Demand (MW)	TSS1	31.9	31.9	31.3	29.1
	TSS2	17.4	16.7	17.1	16.7
	TSS3	31.6	31.6	31.2	30.5
	Total	**80.9**	**80.2**	**79.6**	**76.3**
Energy Loss (MWh)	Total	–	**3.6**	**5.9**	**1.9**
Device Number	SPC	0	0	2	2
	TSESS	0	3	3	1
	Total	**0**	**3**	**5**	**3**

The proposed RBEUS uses two SPCs to transfer RBE for adjacent TSS utilization and recycles RBE by a TSESS, which decreases the returned RBE by about 28.1MWh (about 90.1%). Due to this solution only transfers the RBE between two adjacent TSSs and shares a TSESS, it achieves the best performance in energy loss (about 1.9MWh) and tractive energy reduction (about 26.2MWh). Considering that the grid power demand of the central TSS is significantly lower than that of the other two TSSs, peak-shaving for the two sides of the TSSs is realized by the RBEUS. As a result, the maximum power demand of the three TSSs is significantly decreased by 4.6MW.

Comparison show that the proposed RBEUS achieves comprehensive and excellent performance in RBE utilization, tractive energy reduction, and maximum power demand shaving. More importantly, the proposed RBEUS separately reduces two ESSs and two TSESSs compared to Scheme I and Scheme II. Thus, the proposed RBEUS provides a superior solution compared to existing methods in the literature.

V. DISCUSSION

Based on the comprehensive verification above, the superior performance of the RBEUS has been testified. However, fault protection and economy are critical for the practical implementation of the RBEUS, which will be discussed in this section.

A. Fault Protection

Fault protection for the RPS integrated with the RBEUS involves two aspects: self-protection of the RBEUS and coordinated protection between the RBEUS and the RPS. The self-protection of the RBEUS involves converter protection and relay protection for SPCs and TSESS. The coordinated protection between the RBEUS and the RPS aims to coordinate the time delay of their relay protection to protect the RBEUS and RPS to avoid being affected by the faults from the other one. In order to ensure the reliability of the relay protection of the RPS, the relay protection setting of the RBEUS should be less than the RPS. In this context, the RBEUS can first disconnect from the RPS in fault conditions.

If the fault occurs in the RPS (such as the catenary ground fault), the self-protection of the RBEUS can firstly block the control pulses for converters within two control cycles after detecting the severe fault signal (the converter control frequency is usually over 2kHz, and the fault detection and control pulses block can be completed within 1ms). Then, the relay protection needs a time delay with several dozens of milliseconds to disconnect the RBEUS from the catenary. The RBEUS can be firstly disconnected from the catenary after the fault because the time delay of the relay protection is shorter than the RPS. After that, the relay protection of the RPS can accurately handle the RPS fault. As a result, the RBEUS will not aggravate the fault because it stops operation after blocking the control pulses. Moreover, the RBEUS protection relies on the local protection systems of the SPC and TSESS, which are not affected by communication. Under this protection framework, the RBEUS and the RPS can safely operate in the complex operation conditions of the RPS.

B. Economy

RBE utilization can improve the energy efficiency of the RPS and may support the railway system in being an important actor in the electricity market by selling surplus energy to the power grid or reducing the energy purchases following market price variations in the electricity market [14]. Thus, although the RBEUS brings additional costs for railway operators, it offers economic benefits based on its technical solution in RBE utilization. The economic performance of the RBEUS can be evaluated by its techno-economic model derived from [25]. Specifically, the technical model for the RBEUS can be obtained in (2)-(15) of Section II, and the economic model can be derived from [25] by considering the cost and benefit brought by SPCs additionally. As a result, the techno-economic model for the RBEUS is obtained.

According to the techno-economic model of the RBEUS and [25], the economic performance of the RBEUS and literature methods can be evaluated based on their technical solutions in Table III. The detailed economic parameters for evaluation are from Table II and Table III of [25], and the results are shown in Fig.13. The results show that the net lifetime benefits of the three methods separately are -3022.2k$, 1581.7k$, and 9692.1k$, and the RBEUS only requires three years to return the investment. Therefore, the proposed RBEUS is more economic than literature methods in [9] and [20].

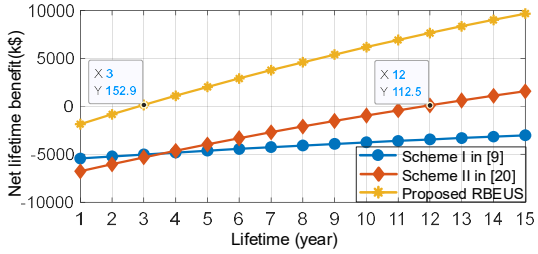

Fig.13 Net lifetime benefits for the RBEUS and literature methods.

The application scenario is a critical influence for the economic performance in the industrial application. The proposed RBEUS is suitable for the three TSSs that return abundant RBE to the power grid, especially for the load powers of each adjacent two TSSs are significantly complementary. Generally, the hub-TSSs and TSSs on the long ramp generate abundant RBE by frequent braking. For the TSSs located in the long ramp (such as the three TSSs of Shenshuo railway used for comparative analysis in Section IV), the trains generate abundant RBE at the downhill direction and consume considerable tractive energy in the inverse direction. Thus, load powers of adjacent TSSs located in the long ramp behave significantly complementary characteristics. Based on this characteristic, the proposed RBEUS can firstly transfer the RBE for adjacent TSS utilization, and then the rest of RBE can be stored by the TSESS in the central TSS. This solution can utilize the RBE by power delivery as much as possible, and the power and energy capacity of the ESS can be reduced. The technical analysis results in Section IV and economic analysis results in this section prove the superiority of the proposed RBEUS.

In recent years, the RPC, SPC, and TSESS have been realized industrial applications in Japan and China [31], [32]. Additionally, the communication system used to control the RBEUS is already available at most modern electrified railways [30]. Therefore, the proposed RBEUS is feasible and promising for implementation from safety, and technical and economic performance.

VI. Conclusion

This paper proposes an integrated RBEUS to achieve RBE coordinated utilization in three consecutive TSSs of the electrified railway via power-sharing and storage. A hierarchically coordinated control strategy is developed to address the real-time control issue of the RBEUS based on its operation principles. It performs centralized management in the system layer based on local data to achieve the optimal power flow by considering the load power, transmission loss, and converter loss. In the converter layer, real-time power flow control of the RBEUS is implemented via decentralized control of the SPCs and TSESS. The proposed RBEUS and control strategy are validated by the HIL-based experiment, which exhibits good performance in RBE utilization and power quality improvement under different operation conditions of the RPS. Besides, a comparison of the proposed RBEUS and literature methods is performed based on the field load data, highlighting the superior performance of the proposed RBEUS. Moreover, the practical implementation of the RBEUS is discussed from the perspectives of fault protection and economy, which shows that the proposed RBEUS provides a practical and feasible solution for RBE utilization in electrified railways.

Appendix

The specific expression of $h(\mathbf{x})$ and $g(\mathbf{x})$ in (17) are given in (A1)-(A3).

$$h(\mathbf{x}) = E_{\mathrm{SC}}(t) - (1-\eta_{\mathrm{sds}})E_{\mathrm{SC}}(t-1) - \Delta t x_3 \tag{A1}$$

$$g(\mathbf{x}) = [g_1(\mathbf{x}), g_2(\mathbf{x}), g_3(\mathbf{x}), g_4(\mathbf{x})]^{\mathrm{T}} \tag{A2}$$

$$\begin{cases} g_1(\mathbf{x}) = [-S^{\mathrm{N}}_{\mathrm{spc1}}, -S^{\mathrm{N}}_{\mathrm{spc2}}, -P^{\mathrm{N}}_{\mathrm{SC}}]^{\mathrm{T}} - [x_1, x_2, x_3]^{\mathrm{T}} \\ g_2(\mathbf{x}) = [-S^{\mathrm{N}}_{\mathrm{spc1}}, -S^{\mathrm{N}}_{\mathrm{spc2}}, -P^{\mathrm{N}}_{\mathrm{SC}}]^{\mathrm{T}} + [x_1, x_2, x_3]^{\mathrm{T}} \\ g_3(\mathbf{x}) = E^{\mathrm{N}}_{\mathrm{ESS}}\mathrm{SoC}_{\mathrm{L}} - (1-\eta_{\mathrm{sds}})E_{\mathrm{ESS}}(t-1) - \Delta t x_3 \\ g_4(\mathbf{x}) = (1-\eta_{\mathrm{sds}})E_{\mathrm{ESS}}(t-1) - E^{\mathrm{N}}_{\mathrm{ESS}}\mathrm{SoC}_{\mathrm{H}} + \Delta t x_3 \end{cases} \tag{A3}$$

The specific expressions of $h(\mathbf{x}^k)$, $g(\mathbf{x}^k)$, $\nabla h(\mathbf{x}^k)$, $\nabla g(\mathbf{x}^k)$ and $\mathbf{H}^k$ are given in (A4)-(A8).

$$h(\mathbf{x}^k) = E_{\mathrm{SC}}(t) - (1-\eta_{\mathrm{sds}})E_{\mathrm{SC}}(t-1) - \Delta t x_3^k \quad \text{(A4)}$$

$$g(\mathbf{x}^k) = [g_1(\mathbf{x}^k), g_2(\mathbf{x}^k), g_3(\mathbf{x}^k), g_4(\mathbf{x}^k)]^{\mathrm{T}} \quad \text{(A5)}$$

$$\nabla h(\mathbf{x}^k) = \nabla(E_{\mathrm{SC}}(t) - (1-\eta_{\mathrm{sds}})E_{\mathrm{SC}}(t-1) - \Delta t x_3^k) \quad \text{(A6)}$$

$$\nabla g(\mathbf{x}^k) = [\nabla g_1(\mathbf{x}^k), \nabla g_2(\mathbf{x}^k), \nabla g_3(\mathbf{x}^k), \nabla g_4(\mathbf{x}^k)]^{\mathrm{T}} \quad \text{(A7)}$$

$$\mathbf{H}^k = \nabla^2 f(\mathbf{x}^k) = \begin{bmatrix} \frac{\partial^2 f}{\partial (x_1^k)^2} & \frac{\partial^2 f}{\partial x_1^k \partial x_2^k} & \frac{\partial^2 f}{\partial x_1^k \partial x_3^k} \\ \frac{\partial^2 f}{\partial x_2^k \partial x_1^k} & \frac{\partial^2 f}{\partial (x_2^k)^2} & \frac{\partial^2 f}{\partial x_2^k \partial x_3^k} \\ \frac{\partial^2 f}{\partial x_3^k \partial x_1^k} & \frac{\partial^2 f}{\partial x_3^k \partial x_2^k} & \frac{\partial^2 f}{\partial (x_3^k)^2} \end{bmatrix} \quad \text{(A8)}$$

REFERENCES

[1] Y. Jiang, J. Liu, W. Tian, M. Shahidehpour, and M. Krishnamurthy, "Energy Harvesting for the Electrification of Railway Stations: Getting a charge from the regenerative braking of trains.A," *IEEE Electrif. Mag*., vol. 2, no. 3, pp. 39-48, Sept. 2014.

[2] K. Minaminosono, M. Hashimoto, and T. Yoshinaga, "Study of Potential and Utilization of Regenerative Power in Electric Railway," *in Proc. 8th Int. Conf. Renew. Energy Res. and Appl. (ICRERA)*, pp. 164-168, 2019.

[3] K. Wang, H. Hu, J. Chen, J. Zhu, X. Zhong, and Z. He, "System-Level Dynamic Energy Consumption Evaluation for High-Speed Railway," *IEEE Trans. Transp. Electrif.,* vol. 5, no. 3, pp. 745-757, Sep. 2019.

[4] H. Hu, Z. He, K. Wang, X. Ma, and S. Gao, "Power-quality impact assessment for high-speed railway associated with high-speed trains using train timetable—part II: Verifications, estimations and applications," *IEEE Trans. Power Del.*, vol. 31, no. 4, pp. 1482–1492, Aug. 2016

[5] A. Frilli, E. Meli, D. Nocciolini, L. Pugi, and A. Rindi, "Energetic optimization of regenerative braking for high speed railway systems," *Energy Convers. Manage.,* vol. 129, pp. 200-215, Dec. 2016.

[6] M. Khodaparastan, A. A. Mohamed, and W. Brandauer, "Recuperation of Regenerative Braking Energy in Electric Rail Transit Systems," *IEEE Trans. Intell. Transp. Syst.,* vol. 20, no. 8, pp. 2831-2847, Aug. 2019.

[7] H. Hayashiya *et al.*, "Possibility of energy saving by introducing energy conversion and energy storage technologies in traction power supply system," in *Proc. 15th Eur. Conf. Power Electro. Appl.,* 2013, pp. 1-8.

[8] J. C. Hernandez and F. S. Sutil, "Electric Vehicle Charging Stations Feeded by Renewable: PV and Train Regenerative Braking," *IEEE Lat. Am. Trans.,* vol. 14, no. 7, pp. 3262-3269, July 2016.

[9] J. Chen, H. Hu, Y. Ge, K. Wang, W. Huang, and Z. He, "An Energy Storage System for Recycling Regenerative Braking Energy in High-Speed Railway," *IEEE Trans. Power Del.,* vol. 36, no. 1, pp. 320-330, Feb. 2021.

[10] E. Pilo de la Fuente, S. K. Mazumder, and I. G. Franco, "Railway Electrical Smart Grids: An introduction to next-generation railway power systems and their operation," *IEEE Electrif. Mag.,* vol. 2, no. 3, pp. 49-55, Sept. 2014.

[11] M. Brenna, F. Foiadelli, and H. J. Kaleybar, "The Evolution of Railway Power Supply Systems Toward Smart Microgrids: The concept of the energy hub and integration of distributed energy resources," *IEEE Electrif. Mag.,* vol. 8, no. 1, pp. 12-23, Mar. 2020.

[12] E. Pilo, S. K. Mazumder, and I. Gonzalez-Franco, "Smart Electrical Infrastructure for AC-Fed Railways With Neutral Zones," *IEEE Trans. Intell. Transp. Syst.,* vol. 16, no. 2, pp. 642-652, Apr. 2015.

[13] Z. Gao, Q. Lu, C. Wang, J. Fu, and B. He, "Energy-Storage-Based Smart Electrical Infrastructure and Regenerative Braking Energy Management in AC-Fed Railways with Neutral Zones," *Energies,* vol. 12, no. 21, pp. 4053-4076, Nov. 2019.

[14] S. Khayyam, F. Ponci, J. Goikoetxea, V. Recagno, V. Bagliano, and A. Monti, "Railway Energy Management System: Centralized–Decentralized Automation Architecture," *IEEE Trans. Smart Grid,* vol. 7, no. 2, pp. 1164-1175, Mar. 2016.

[15] S. Khayyam, N. Berr, L. Razik, M. Fleck, F. Ponci, and A. Monti, "Railway System Energy Management Optimization Demonstrated at Offline and Online Case Studies," *IEEE Trans. Intell. Transp. Syst.,* vol. 19, no. 11, pp. 3570-3583, Nov. 2018.

[16] M. Chen, Z. Cheng, Y. Liu, Y. Cheng, and Z. B. Tian, "Multitime-Scale Optimal Dispatch of Railway FTPSS Based on Model Predictive Control," *IEEE Trans. Transp. Electrif.,* vol. 6, no. 2, pp. 808-820, Jun. 2020.

[17] I. Sengor, H. C. Kilickiran, H. Akdemir, B. Kekezoglu, O. Erdinc, and J. P. S. Catalao, "Energy Management of a Smart Railway Station Considering Regenerative Braking and Stochastic Behaviour of ESS and PV Generation," *IEEE Trans. Sustain. Energy,* vol. 9, no. 3, pp. 1041-1050, Jul. 2018.

[18] L. Jiang, Z. Bie, T. Long, H. Xie, and Y. Xiao, "Distributed energy management of integrated electricity-thermal systems for high-speed railway traction grids and stations," *CSEE J. Power Energy Syst*, vol. 7, no. 3, pp. 541-554, May 2021.

[19] V. A. Morais, J. L. Afonso, and A. P. Martins, "Towards Smart Railways: A Charging Strategy for Railway Energy Storage Systems," *EAI Endorsed Trans. on Energy Web*, pp. 1–17, Jan. 2021.

[20] Q. Lu, Z. Gao, B. He, C. Che, and C. Wang, "Centralized-Decentralized Control for Regenerative Braking Energy Utilization and Power Quality Improvement in Modified AC-Fed Railways," *Energies,* vol. 13, no. 10, pp. 2582-2612, May 2020.

[21] P. Xie et al., "Optimization-Based Power and Energy Management System in Shipboard Microgrid: A Review," *IEEE Syst. J.*, to be published.

[22] H. Jafari Kaleybar, H. Madadi Kojabadi, S. Saeed Fazel, and F. Foiadelli, "An intelligent control method for capacity reduction of power flow controller in electrical railway grids," *Electr. Power Syst. Res.,* vol. 165, pp. 157-166, 2018.

[23] I. Perin, G. R. Walker, and G. Ledwich, "Load sharing and wayside battery storage for improving AC railway network performance with generic model for capacity estimation, Part 1," *IEEE Trans. Ind. Electron.*, vol. 66, no. 3, pp. 1791-1798, Mar. 2019.

[24] I. Perin, G. R. Walker, and G. Ledwich, "Load sharing and wayside battery storage for improving AC railway network performance with generic model for capacity estimation, Part 2," *IEEE Trans. Ind. Electron.*, vol. 65, no. 12, pp. 9459-9467, Dec. 2018.

[25] J. Chen, H. Hu, Y. Ge, K. Wang, and Z. He, "Techno-Economic Model-Based Capacity Design Approach for Railway Power Conditioner-Based Energy Storage System," *IEEE Trans. Ind. Electron.*, vol. 69, no. 5, pp. 4730-4741, May 2022.

[26] Y. Mochinaga, M. Takeda, and K. Hasuike, "Static power conditioner using GTO converters for ac electric railway," in *Conf. Rec. Power Conversion Conf., Yokohama*, Japan, pp. 641–646, Apr. 1993.

[27] H. Hajebrahimi, S. M. Kaviri, S. Eren, and A. Bakhshai, "A New Energy Management Control Method for Energy Storage Systems in Microgrids," *IEEE Trans. Power Electron.,* vol. 35, no.11, pp. 11612-11624, Nov. 2020.

[28] Boggs, Paul T., and Jon W. Tolle. "Sequential quadratic programming." Acta numerica 4: 1-51, 1995.

[29] C H. Naga Sai Kalyan and G. Sambasiva Rao. "Impact of communication time delays on combined LFC and AVR of a multi-area hybrid system with IPFC-RFBs coordinated control strategy," *Protection and Control of Modern Power Systems*, vol. 6, no. 1, pp. 89-108, 2021.

[30] J. Zhu, H. Hu, Z. He, et al. "A power-quality monitoring and assessment system for high-speed railways based on train-network-data center integration," *Rail. Eng. Science*, vol. 29, pp. 30–41, Mar. 2021.

[31] M. Ohmi and Y. Yoshii, "Validation of Railway Static Power Conditioner in Tohoku Shinkansen on actual operation," in *the 2010 International Power Electronics Conference - ECCE ASIA*, pp. 2160-2164, 2010.

[32] D. Zhang, Z. Zhang, W. Wang, and Y. Yang, "Negative Sequence Current Optimizing Control Based on Railway Static Power Conditioner in V/v Traction Power Supply System," *IEEE Trans. Power Electron.,* vol. 31, no. 1, pp. 200-212, Jan. 2016.

Junyu Chen (Student Member, IEEE) received the B.S. degree in electrical engineering from the Chengdu University of Technology, Chengdu, China, in 2017. He is currently pursuing the Ph.D. degree in electrical engineering at Southwest Jiaotong University, Chengdu.

His current research interests include the regenerative braking energy utilization, modeling, control, and application of the energy storage systems in the electrified railway.

Yinbo Ge (Student Member, IEEE) received the B.S. degree in electrical engineering from Southwest Jiaotong University, Emei, China, in 2017. He is currently pursuing the Ph.D. degree in electrical engineering at Southwest Jiaotong University, Chengdu.

His current research interests include power converters control, integration of renewable energy source and energy storage systems, and energy management strategy of electric traction system.

Ke Wang (Member, IEEE) received the B.S. degree from South-west Jiaotong University, Emei, China, in 2011 and the M.Sc. degree, Ph.D degree from Southwest Jiaotong University, Chengdu, China, in 2015 and 2020, all in electrical engineering.

He is currently a Postdoctoral Researcher in the School of Electrical Engineering at Southwest Jiaotong University. His main research interests are energy consumption evaluation, power quality, and harmonics of the electric traction system.

Haitao Hu (Senior Member, IEEE) received the B.S. degree from Zhengzhou University, Zhengzhou, China, in 2010, and the Ph.D. degree from Southwest Jiaotong University, Chengdu, China, in 2014, all in electrical engineering.

He is currently a Professor in the School of Electrical Engineering at Southwest Jiaotong University. His main research interests are power quality and stability of the electric traction system.

He received the 2017 outstanding reviewer award of IEEE Transactions on Power Delivery, and 2018 outstanding reviewer of International Journal of Electrical Power and Energy Systems. He serves as an Associate Editor for the Journal of Modern Power Systems and Clean Energy (MPCE).

Zhengyou He (Senior Member, IEEE) received the B.Sc. degree and M. Sc. degree in Computational Mechanics from Chongqing University, Chongqing, China, in 1992 and 1995, respectively. He received the Ph.D. degree in the School of Electrical Engineering from Southwest Jiaotong University, Chengdu, China, in 2001.

He is currently a Professor in the School of Electrical Engineering at Southwest Jiaotong University. His research interests include signal process and information theory applied to power systems, and the application of wavelet transforms in power systems.

Zhongbei Tian (Member, IEEE) received the B.Eng in Huazhong University of Science and Technology, Wuhan, China, in 2013. He received the B.Eng. and PhD degree in Electrical and Electronic Engineering from the University of Birmingham, Birmingham, U.K., in 2013 and 2017.

He is currently a Lecturer in Electrical Energy Systems at the University of Liverpool. His research interests include railway traction power system modeling and analysis, energy-efficient train control, energy system optimization, and sustainable transport energy systems integration and management.

Yunwei Li (Fellow, IEEE) received the B. Sc. in Engineering degree in electrical engineering from Tianjin University, Tianjin, China, in 2002, and the Ph.D. degree from Nanyang Technological University, Singapore, in 2006. In 2005, he was a Visiting Scholar with Aalborg University, Aalborg, Denmark. From 2006 to 2007, he was a Postdoctoral Research Fellow with Ryerson University, Toronto, ON, Canada. In 2007, he was with Rockwell Automation, Cambridge, ON, Canada, before he joined the University of Alberta, Edmonton, AB, Canada; since then, he has been with the University of Alberta, where he is currently a Professor. His research interests include distributed generation, microgrid, renewable energy, high-power converters, and electric motor drives.

Dr. Li serves as an Editor-in-Chief of the IEEE Transactions on Power Electronics Letters. He was an Associate Editor for the IEEE Transactions on Power Electronics, IEEE Transactions on Industrial Electronics, IEEE Transactions on Smart Grid, and IEEE Journal of Emerging and Selected Topics in Power Electronics. He was the recipient of the Richard M. Bass Outstanding Young Power Electronics Engineer Award from IEEE Power Electronics Society in 2013 and the Second Prize Paper Award of IEEE Transactions on Power Electronics in 2014. He is listed as a Highly Cited Researcher by the Web of Science Group.